Time-Dependent Boundary-Layer Response in a Propeller Slipstream

Richard M. Howard*
U.S. Naval Postgraduate School, Monterey, California
and
Stan J. Miley†
Texas A&M University, College Station, Texas

The time-dependent behavior of a wing boundary layer immersed in a propeller slipstream has been studied experimentally in wind-tunnel tests and in flight. Hot-wire anemometer measurements were made through the boundary layer for time-dependent, ensemble-average velocity and turbulence-intensity profiles at various chord locations. The boundary layer has a coherent, time-dependent cycle of transitional behavior, varying from a laminar to a turbulent-transitional state. Local drag coefficients determined from the velocity profiles for the freewheeling propeller case in flight show that the time-dependent drag in the propeller slipstream varies from the undisturbed laminar value to a value less than that predicted for fully turbulent flow. Local drag coefficients determined from the thrusting propeller case in the wind tunnel indicate that the effects of the slipstream are to enhance the stability of the boundary layer and to reduce the drag coefficient in the laminar portion of the cycle below its undisturbed laminar value.

Nomenclature

C_d = airfoil sectional-profile drag coefficient
C_{dx} = Squire–Young sectional-profile drag coefficient to station x
C_{dxo} = Squire–Young sectional-profile drag coefficient to station x for undisturbed laminar flow
C_p = pressure coefficient $= [p - p_\infty]/q_\infty$
c = airfoil chord
H_{12} = boundary-layer momentum thickness parameter $= \delta_1/\delta_2$
J = propeller advance ratio
L = upper surface arclength from leading edge to trailing edge
l = reference length of flow
p = static pressure
q_∞ = freestream dynamic pressure
R = propeller radius
Re_c = chord Reynolds number $= U_\infty c/\nu$
Re_x = Reynolds number to station x
r = radial station along propeller radius
S = upper surface arclength to station x
Tu = measured turbulence intensity $= \sqrt{(u')^2}/U_e$
U = streamwise mean or ensemble-average velocity
$\underline{u}$ = streamwise instantaneous velocity
$(u')^2$ = mean square of the fluctuating velocity
V = transverse mean velocity
v = transverse instantaneous velocity
x = streamwise coordinate
y = transverse coordinate
δ = boundary-layer thickness
δ_1 = boundary-layer displacement thickness, $\int_0^\infty [1 - (U/U_e)]\, dy$
δ_2 = boundary-layer momentum thickness, $\int_0^\infty (U/U_e)[1 - (U/U_e)]\, dy$
ν = kinematic viscosity of air

Subscripts

e = boundary-layer edge value
∞ = freestream value

Superscripts

$'$ = fluctuating quantity
$\overline{\ }$ = time mean value

Introduction

PRIOR to World War II, the propeller slipstream was generally considered to be highly turbulent and to result in increased friction drag over the wing. Young and Morris[1,2] and Hood and Gaydos[3] concluded that the propeller slipstream caused the point of transition to turbulent flow to move forward to a point near the wing leading edge. Flight tests by Zalovcik[4] and Zalovcik and Skoog[5] using an NACA 66 series airfoil indicated a movement forward of the transition point from 50 to 20% chord. The general consensus from this early work was that the propeller slipstream reduced the extent of laminar flow by forcing transition to occur earlier.

Recent studies have shown the wing boundary layer to respond periodically to the cyclic turbulence of the propeller blade wake. Holmes et al.[6] made surface hot-film measurements on a wing in the propeller slipstream, which indicated the existence of a cyclic turbulent behavior of the boundary layer. Miley et al.[7] performed wind-tunnel measurements of boundary-layer velocity profiles on a slipstream-immersed wing and showed similarities through shape-factor correlations between these profiles and those of relaminarizing boundary layers, and those of low-Reynolds-number laminar boundary layers with high freestream turbulence.

A more complete wind-tunnel investigation has been carried out, as well as flight tests in which hot-wire measurements were made on a laminar-flow wing glove behind a freewheeling propeller. Time-ensemble velocity and turbulence-intensity profiles were constructed from the recorded time-dependent data. The velocity profiles were integrated to determine

Received June 25, 1988; revision received Nov. 21, 1988.

*Assistant Professor, Department of Aeronautics and Astronautics. Member AIAA.

†Associate Professor, Aerospace Engineering Department; currently, Guest Scientist, Institut für Entwurfsaerodynamik, DFVLR, Braunschweig, West Germany. Member AIAA.

Squire–Young[8] drag coefficients for comparison to the undisturbed laminar flow case and the case for a fully turbulent (forced transition near the leading edge) boundary layer.

Experiments

Wind-Tunnel Tests

Wind-tunnel experiments were performed in the Texas A&M University 2- × 3-ft low-speed wind tunnel. The wind tunnel is of the closed-circuit type and has an ambient turbulence level of 0.3% intensity at test conditions. The test model was a 30-in. chord NACA 0012 wing section with an 18-in. diam propeller and electric motor mounted at wing level 1/5-chord distance upstream of the wing leading edge. A two-bladed variable-pitch propeller with no twist was used. The propeller blade pitch angle was set to minimize the length of the turbulent pulse in the resulting wake; the blade pitch angle was set at 23 deg for the low-speed case and at 40 deg for the high-speed case, providing positive thrust coefficients. Test chord Reynolds numbers were 0.6 and 1.2×10^6, and rotation speeds treated were 20 and 25 Hz (1200 and 1500 rpm).

A hot-film anemometer probe was traversed throughout the boundary layer to acquire instantaneous velocity data over a long period of time for ensemble averaging and construction of time-dependent profiles. As the flight measurements would require data to be stored in analog form on magnetic tape, the same storage system was used in the wind-tunnel experiments rather than storing directly with a microcomputer. This process allowed for a validation of the software and hardware to be used for the flight experiments. A one-per-revolution signal from a proximity transducer was also recorded to allow for proper ensemble averaging at the same position in time in the blade-wake passage cycle on each pass. Fifty blade passage cycles were recorded for each test condition; this limit was driven by flight considerations, but 50 passes were determined to be sufficient for the purpose of ensemble averaging the time-dependent data. The data were digitized at 15 kHz, resulting in approximately 800 points per passage cycle. The points in each cycle were divided into 40 groups, and the points in each group were fitted with a local linear least-squares fit. The average value for each group was taken to be the average value of the linear fit, and the rms (root-mean-square) velocity for each group was the average of the local rms values. These values were then averaged over the 50 cycles. In this manner, 40 points were taken across each blade-wake passage cycle with ensemble-average ("mean") velocity and rms profiles at each of the 40 points. Representative profiles are shown in the Results section. An improved data analysis procedure for unsteady turbulence measurements is given by Johnson.[9]

A vertical traversing mechanism was devised to be used in the wind tunnel and in flight. The unit used a stepper motor to operate an offset cam, which allowed a pivot arm to move the probe throughout the boundary layer in a sinusoidal manner, clustering points near the surface. Velocity data were recorded at 48 points in the boundary layer. Hot-film measurements were made at the 30% chord location; the probe was located spanwise at two-thirds the radius from the propeller centerline to the tip.

Flight Tests

The flight program involved hot-wire anemometer and surface pressure measurements on a wing glove with a freewheeling propeller installed on a Schweizer SGS 2-32 sailplane. A test aircraft was desired on which slipstream effects on a wing boundary layer could be studied with no effect due to engine acoustic noise and structural vibration. Testing in a flight environment was desired, as significant differences may exist between tests in wind tunnels and in flight due to the differences in the structure of the freestream turbulence in the two regimes.[10] Numerical calculations with a propeller code indicated that the drag effects for a propeller at a cruise power coefficient are similar to those for a freewheeling propeller, which exhibits a slightly negative power coefficient. The wing-glove arrangement mounted on the sailplane is shown in Fig. 1.

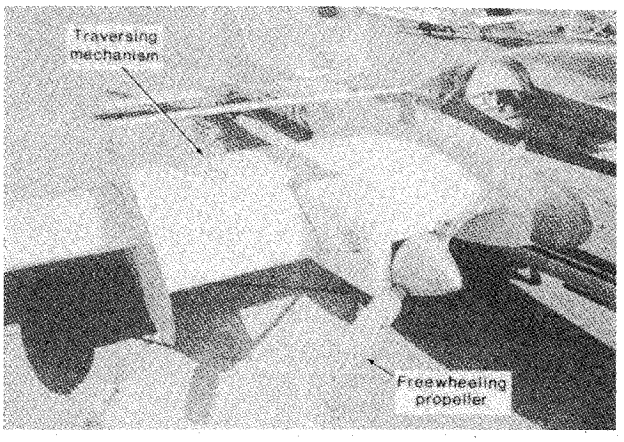

Fig. 1 Wing glove arrangement.

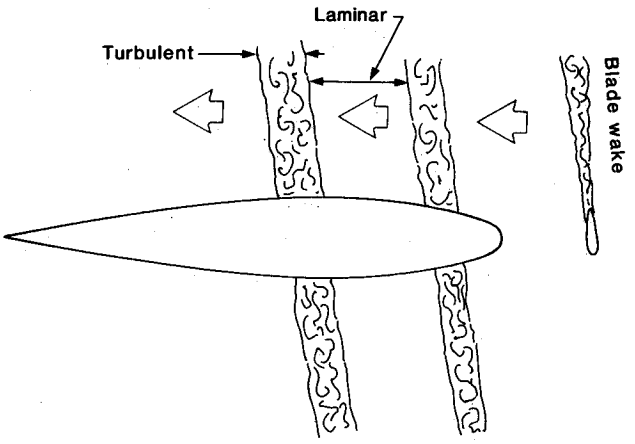

Fig. 2 Slipstream disturbance flow model.

The use of a glove allowed for the construction of a desired airfoil contour and for the measurement of surface pressures. The traversing mechanism moved the hot-wire sensor through the boundary layer at the set chord location. Pressure and hot-wire signals were recorded on magnetic tape with a four-channel FM recorder and were later digitized. For a more complete description of the experimental procedures and the data and error analysis, see Ref. 11.

Results

The flow was considered as a two-dimensional model, as indicated in Fig. 2. The flow varies between a laminar state and a quasiturbulent state at the blade-wake passage frequency when viewed from one station on the wing. (See Ref. 7 for a discussion of previous wind-tunnel tests studying this flowfield.)

Wind-Tunnel Measurements

Hot-film anemometry measurements were made at the 30% chord location. Pressure distributions up to the probe location for four angles of attack (and, therefore, four cases of varying pressure gradient) are shown in Fig. 3. Because of the large relative size of the model in the tunnel, no correlation was attempted between the data for the model and for the NACA 0012; the current tests are considered in terms of pressure gradient rather than in terms of a particular airfoil. Figures 4–6 show the velocity time histories at various points through the boundary layer for three of the cases.

Figure 4 shows the velocity response for the neutral case (case 2) as one moves from the external flow down through the boundary layer to the surface. The two disturbances of the passing blade wake are slightly dissimilar due to a blade-pitch angle difference between the two blades. The relative increase or decrease (velocity deficit) seen in the traces is due to the shift in the shape of the velocity profile. Near the surface, the turbulent profile is fuller and the mean velocity is correspondingly higher than the laminar profile. Away from the surface, the thicker turbulent profile results in a velocity deficit relative to the laminar profile.

In the slightly adverse case (case 3) of Fig. 5, the turbulence remains in the cycle longer due to the less favorable conditions. The adverse pressure gradient makes it difficult for the flow to revert back to the laminar state once the source of the turbulence has passed. Case 4 in Fig. 6 shows the flow to remain almost completely turbulent near the surface due to the adverse gradient. A comparison of the top trace with that of case 2 shows the external flow disturbance to be identical; the width of the external disturbance is little affected by the change in pressure gradient, yet the turbulence production in the boundary layer is very responsive to it. The laminar stability of the boundary layer determines how much of the resulting periodic flow will be turbulent.

The neutral and slightly adverse cases are considered in more detail. Five ensemble-average velocity and turbulence-intensity profiles are shown in Figs. 7 and 8 for one blade passage cycle. For case 2, the stages progress from 1) the laminar with almost no turbulence; 2) to a highly turbulent, with an almost constant level of turbulence intensity across

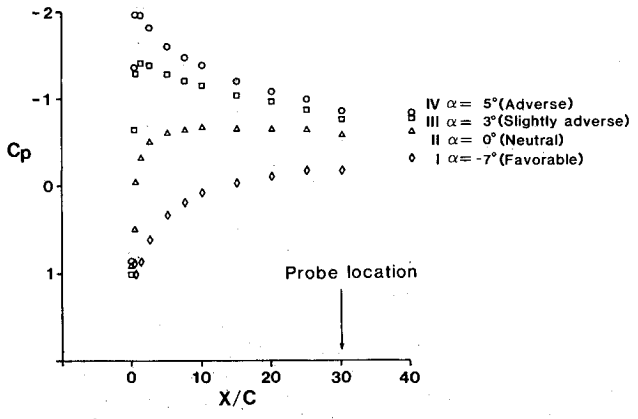

Fig. 3 Pressure distributions for wind-tunnel model.

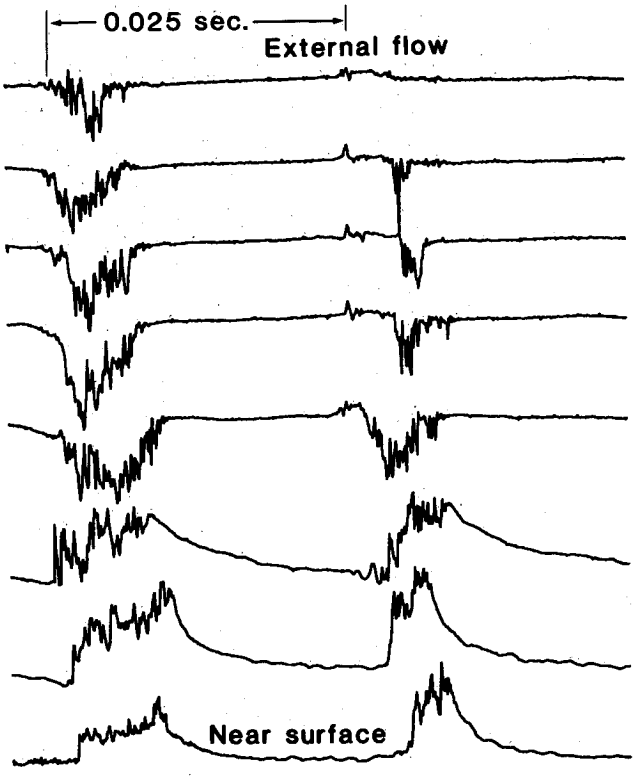

Fig. 4 Velocity time histories in boundary layer; case 2—neutral.

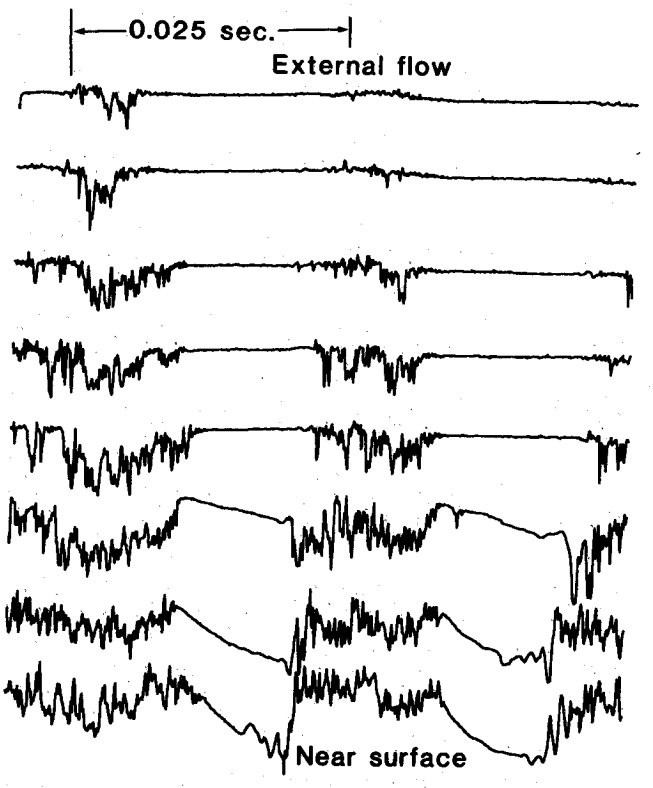

Fig. 5 Velocity time histories in boundary layer; case 3—slightly adverse.

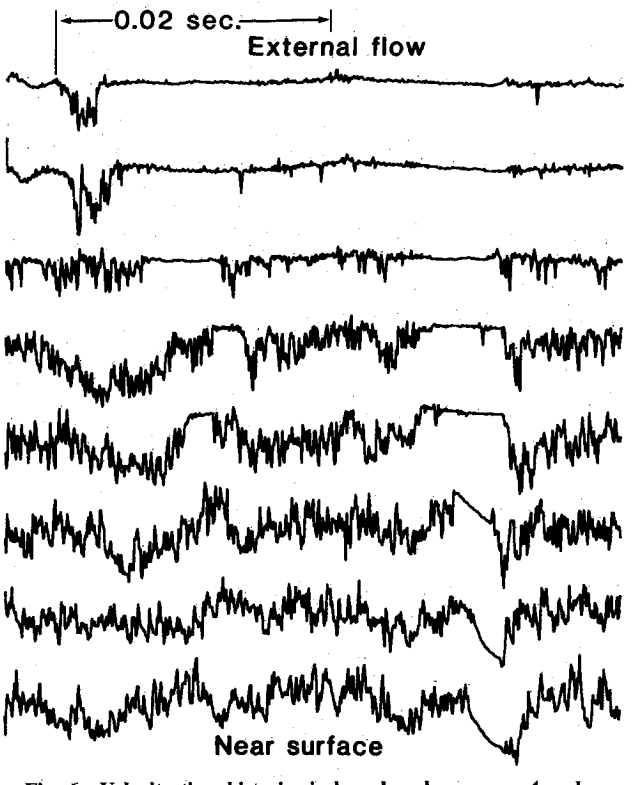

Fig. 6 Velocity time histories in boundary layer; case 4—adverse.

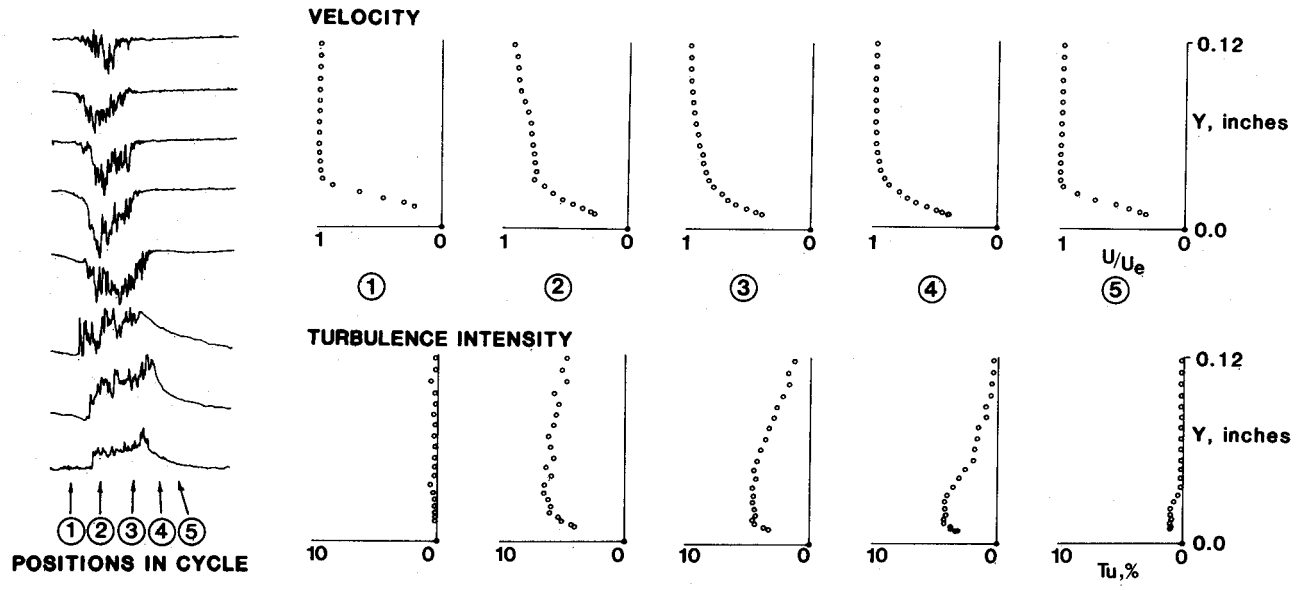

Fig. 7 Ensemble-average profiles; case 2—neutral.

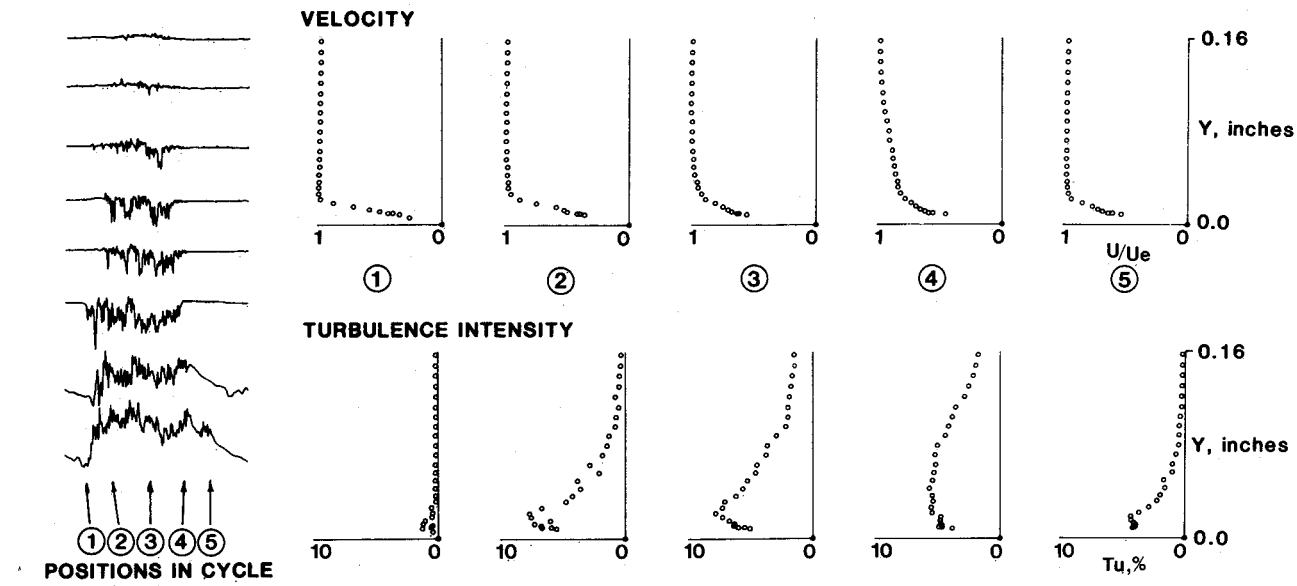

Fig. 8 Ensemble-average profiles; case 3—slightly adverse.

the boundary layer; 3) and 4) to a profile in a relaminarization phase, where a large amount of turbulence is being generated near the surface, though the value of external turbulence is low; and 5) back to the laminar.

The apparent effect of the increased adverse pressure gradient of case 3 is to make the profile much more sensitive to the external disturbance. Note in Fig. 8 in the second profile to what extent the turbulence near the surface has been generated. The time between profiles is of the order of a few milliseconds.

Flight Measurements

Shown in Fig. 9 are pressure distributions for the glove airfoil at various indicated airspeeds. Pressures were measured at a spanwise location of three-quarters the propeller radius and approximately one-half the glove semispan. The presence of the nacelle that housed the propeller shaft and brake mechanism altered the basic airfoil pressure data; no correlation of indicated airspeed with airfoil angle of attack was made. Measurements were made at 10 and 22% chord, and the airspeed range from 60–75 mph IAS resulted in local pressure gradients from favorable to neutral or slightly adverse.

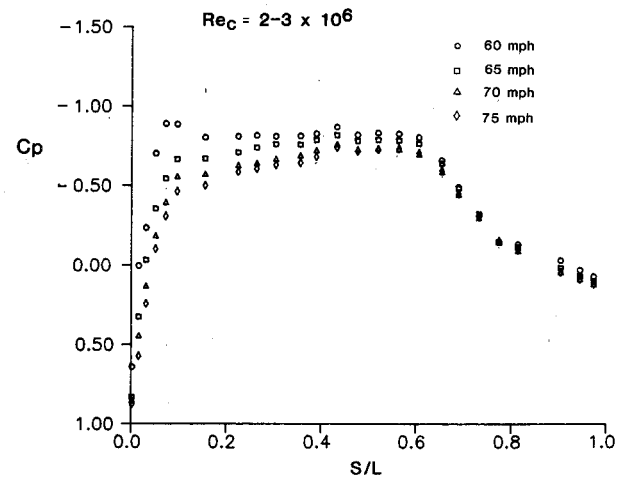

Fig. 9 Pressure distributions on wing glove and nacelle.

Time histories of the boundary-layer response are shown for probe locations at 10 and 22% chord, denoted as cases A

and B, respectively, in Figs. 10 and 11. Only one airspeed result is shown, as the response did not vary significantly over the speed envelope allowed for the instrumented aircraft. The results in Fig. 10 at 10% chord appear to be almost identical to those for the neutral case in the wind-tunnel experiments. For case B at 22% chord, the external flow disturbance is much wider due to the fact that the propeller is freewheeling rather than thrusting.

Shown in Fig. 12 are ensemble-average velocity and turbulence-intensity profiles at 65 mph IAS at 10% chord location. Profiles are shown for the time of one blade-wake passage, as indicated by the positions in the time-history traces at the far left of the figure. Of interest is the amount of turbulence generated near the surface in the second frame; the velocity-profile shape has changed little, yet an intensity of 3% has been generated near the surface. The time between the first and last frames is approximately 20 ms.

Figure 13 shows the same distributions at 22% chord. The velocity profiles are obviously much thicker and the turbulence intensity has greatly increased in the outer layer. A comparison at the two chord locations indicates that, as the flow moves downstream, the location in the boundary layer of maximum turbulence intensity has shifted from the wall and the intensity distribution is fuller across the boundary layer. Such high values of turbulence intensity in the outer layer, where the mean shear stress is low, require a high value of the local eddy or turbulent viscosity. This requirement questions how well an algebraic eddy-viscosity turbulence model might perform in predicting flows with high levels of external turbulence.

Drag Calculations

It was desired to determine drag coefficients, to compare the time-dependent propeller slipstream flow to the fully (steady)

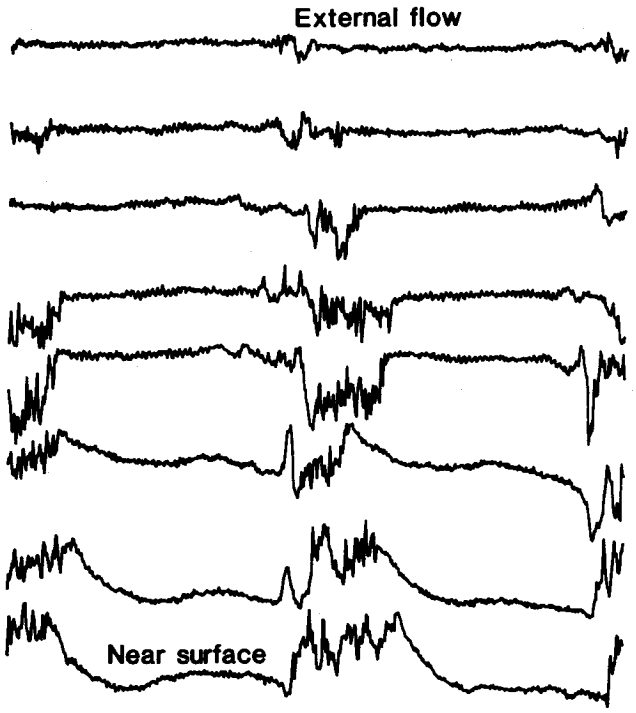

Fig. 10 Velocity time histories in boundary layer; 10% chord.

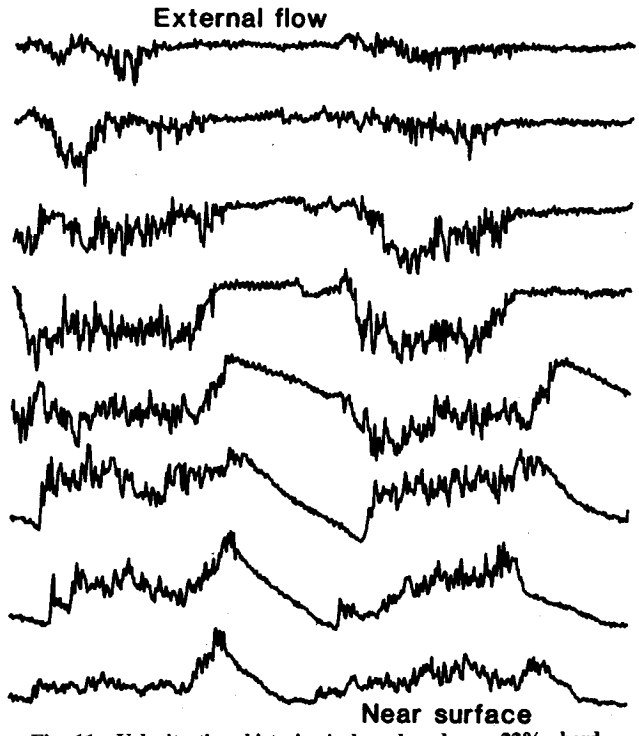

Fig. 11 Velocity time histories in boundary layer; 22% chord.

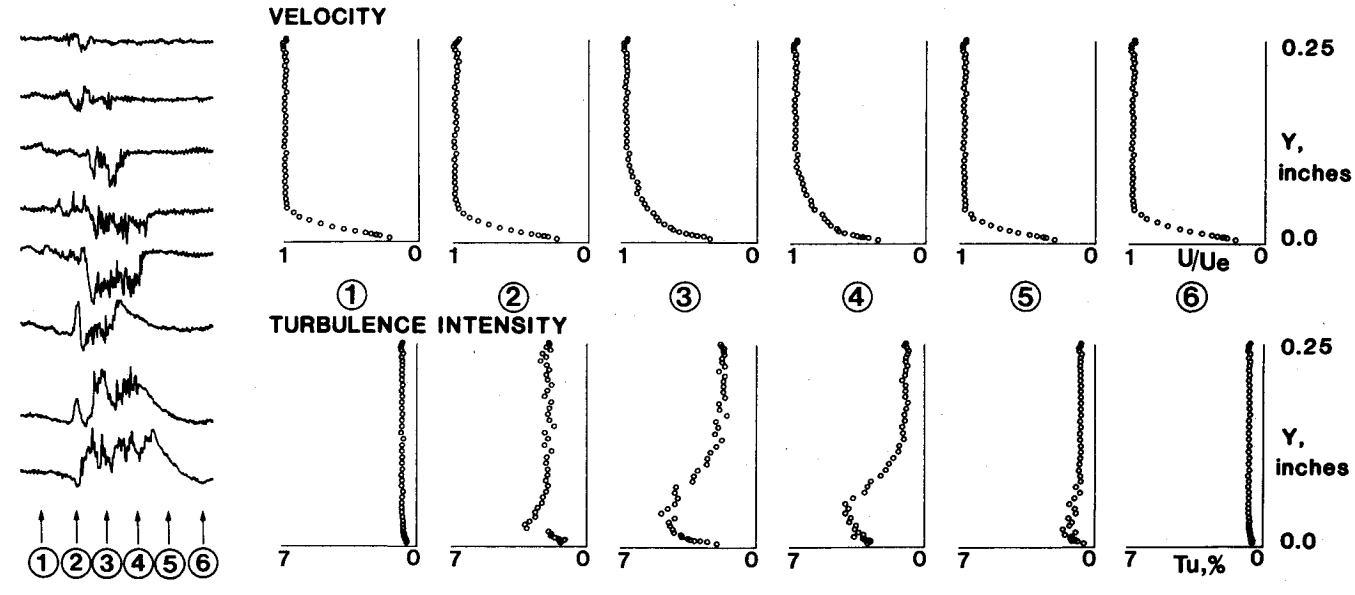

Fig. 12 Ensemble-average profiles; 10% chord, 65 mph IAS.

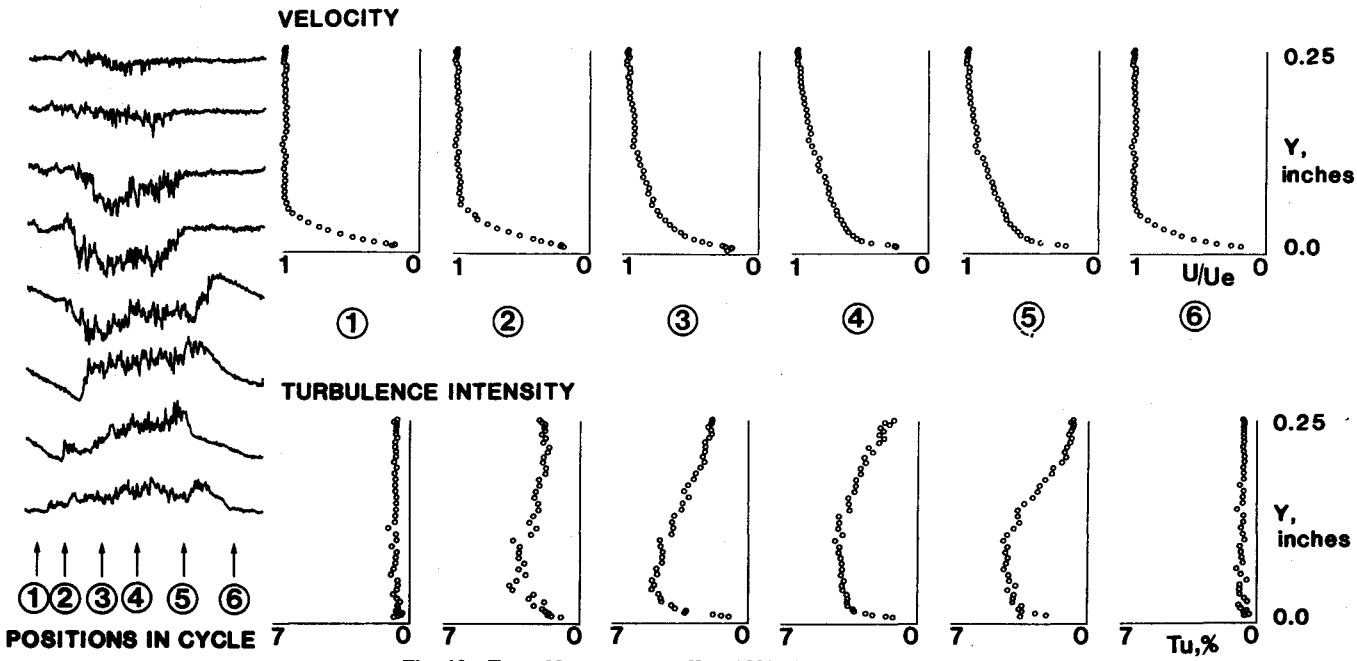

Fig. 13 Ensemble-average profiles; 22% chord, 65 mph IAS.

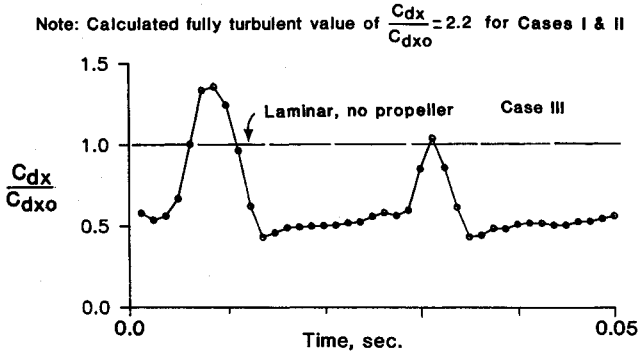

Fig. 14 Profile drag-time history; wind-tunnel model, $Re_x = 6 \times 10^5$, $J = 1.33$.

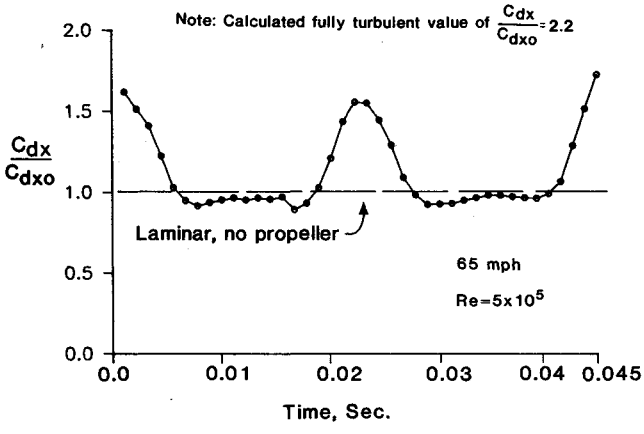

Fig. 15 Profile drag-time history; freewheeling propeller, 10% chord.

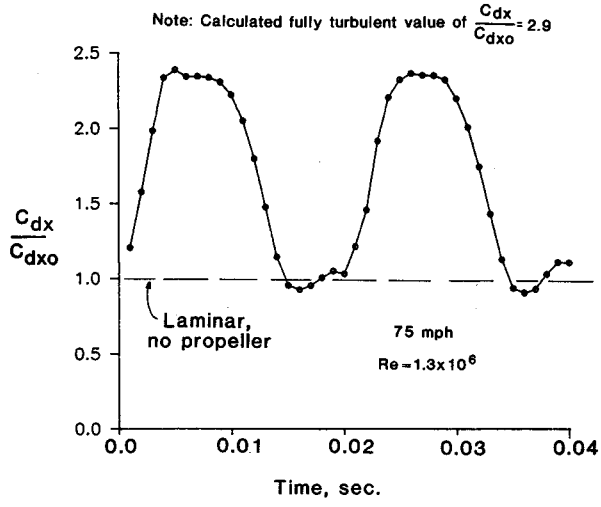

Fig. 16 Profile drag-time history; freewheeling propeller, 22% chord.

laminar and turbulent cases. A means of calculating drag from the time-dependent hot-film measurements was preferred to other experimental methods that give only time-averaged information. A local skin-friction coefficient would be an important parameter to characterize the flow, but no universal relationship between the local skin friction and the general profile shape exists for transitional velocity profiles.

The profile drag coefficient of Squire and Young[8] was chosen for the drag calculations. This drag coefficient is based upon a relation between the drag of a body and the application of the momentum integral equation in the wake far downstream of the body. Originally applied to determine the profile drag for an airfoil by inputting integral parameters found from trailing-edge conditions, the Squire–Young method can be applied to find the profile drag coefficient for a surface up to a particular station. Although not as useful as a local skin-friction coefficient, the Squire–Young profile drag coefficient takes into account the history of a flow up to the point of measurement. The expression is written

$$C_{dx} = 2 \cdot \delta_2/l \cdot [U_e/U_\infty]^{(H_{12}+5)/2}$$

where the momentum thickness δ_2, reference length l, velocity ratio U_e/U_∞, and shape factor H_{12} are taken at the desired location. Forty profiles were determined across one propeller revolution cycle; each profile was numerically smoothed, fit with a cubic spline, and integrated across the boundary layer as necessary to obtain the parameters δ_2 and H_{12}. The same was done for the laminar profile for the test condition with no propeller. This value, denoted C_{dxo}, was used as a reference for the C_{dx} of the time-dependent profiles.

Wind-Tunnel Results

Values of the profile drag coefficient for case 3 are shown in Fig. 14. Cases 1 and 2 show no marked change from case 3 except for the drag peak being slightly lower and the width of the drag rise being slightly narrower. Results for these cases can be found in Ref. 11. Case 4 is not presented as the reference profile was transitionally turbulent. The blade-wake passage frequency was 40 Hz.

The drag-coefficient ratio for the adverse case 3 rises from a level of about 0.5 to 1.4 for one blade and to 1.0 for the other. Of interest is that the drag ratio is one-half that for the no-propeller case for the laminar portion. This reduction was reflected in cases 1 and 2 also, and is in concurrence with the conclusion drawn by Miley et al.[7] that the propeller slipstream may tend to have a beneficial effect in portions of the slipstream periodic cycle. In that reference, it can be noted that an amount of laminar flow existed at 80% chord in the slipstream boundary layer, whereas the flow was fully turbulent with no propeller. Apparently, the slipstream can "carry" laminar flow between the highly turbulent disturbances of the blade wake, and can reduce the drag coefficient in the laminar portion of the cycle.

The value of the drag ratio for a fully turbulent boundary layer (transitioning near the leading edge), as calculated with the boundary-layer method of Cebeci and Carr,[12] is approximately 2.2 for cases 1 and 2. No value for case 3 was available as the code predicted laminar separation to have taken place. The predicted value is well above those data in the turbulent portion of the cycle. This difference supports the statement that the turbulent portion of the boundary layer in the slipstream cycle is reduced in its severity as a turbulent boundary layer.

Apparently, the flow in the propeller slipstream provides an energizing effect that works to enhance the stability of the wing boundary layer.

Flight Results

Profile drag coefficients were determined from the ensemble-average data measured in flight, as was done for the wind-tunnel runs. Again, the no-propeller laminar value was used for the reference value. Sample cases for 65 mph IAS at 10% chord and for 75 mph IAS at 22% chord are shown in Figs. 15 and 16.

The same general behavior observed in the wind tunnel is seen, with one particular difference. In each case, the laminar portion gives a drag ratio of about 1.0, and the turbulent rise reaches a value of between 1.5 and 2.5. In the wind tunnel, the propeller was thrusting; in flight, the propeller is freewheeling. The minimum value of the drag coefficient reached in the slipstream in flight is simply that of the no-propeller, laminar flow situation. Under these conditions, the drag between the turbulent portions of the cycle appears to be no higher than for natural laminar flow. The drag-coefficient plot at the 22% chord position shows a higher value of drag ratio in the turbulent portion, having increased from about 1.6 at 10% chord to 2.4. The plot also shows the high-drag region to remain in the cycle for a much longer time than at 10% chord, correlating with the results of the time histories.

The drag ratios predicted by the Cebeci code for the fully turbulent-to-laminar case for the test conditions are 2.2 for the 65 mph, 10% chord condition and 2.9 for the 75 mph, 22% chord case. In each case, the calculated fully turbulent values are proportionally higher than those determined for the turbulent portion of the actual wake cycle. This result supports the statement that the high external-turbulence boundary layer in the propeller slipstream never behaves as a classical fully turbulent boundary layer. In the propeller slipstream, apparently the boundary layer exposed to high external turbulence levels becomes a highly stable transitional boundary layer, energized by the slipstream flow.

Conclusions

A wind-tunnel and flight investigation was performed to gain an understanding of the physical behavior of the wing boundary layer immersed in the propeller slipstream. Ensemble-average velocity and turbulence-intensity profiles across the boundary layer were determined with a time resolution of less than a millisecond. The profiles at a fixed station vary between laminar, quasiturbulent, and transitional profiles.

Sectional drag coefficients were calculated across the blade-wake passage cycle. The in-flight measurements in the freewheeling propeller cases indicate a periodic drag rise from the undisturbed laminar boundary-layer value to a value less than would exist if the flow were fully tripped to be turbulent from near the leading edge. The thrusting cases from the wind-tunnel tests indicate a similar periodic drag rise, but one returning to a value less than the value for the undisturbed laminar boundary layer. It is supposed that in the thrusting case an energization of the flow is taking place, resulting in a thinner, more stable boundary layer.

The boundary layer is a highly resilient shear flow with the ability to respond in a periodic laminar/turbulent manner to a relatively high-frequency turbulent disturbance. Drag calculations based on ensemble-average velocity profiles indicate a flow whose time-mean drag is well below that for a fully turbulent boundary layer.

Acknowledgments

This work was supported by NASA Langley Research Center through Grant NAG 1-344, with contract monitor Dr. Bruce Holmes. The authors wish to thank Dr. L. Scott Miller, Mr. James Blohowiak, and Ms. Pixey Mosley for their help in carrying out the model construction and the flight tests, and Dr. Donald T. Ward for his role as flight test pilot. The authors also wish to thank the reviewers for their suggestions.

References

[1]Young, A. D. and Morris, D. E., "Note on Flight Tests on the Effect of Slipstream on Boundary Layer Flow," *Aeronautical Research Council R&M*, No. 1957, 1939.

[2]Young, A. D. and Morris, D. E., "Further Note on Flight Tests on the Effect of Slipstream on Boundary-Layer Flow," Royal Aircraft Establishment Rept. No. B.A. 1404b, 1939.

[3]Hood, M. J. and Gaydos, M. E., "Effects of Propellers and Vibration on the Extent of Laminar Flow on the NACA 27-212 Airfoil," NACA ACR (WR L-784), 1939.

[4]Zalovcik, J. A., "Flight Investigation of the Boundary Layer and Profile Drag Characteristics of Smooth Wing Sections on a P-47D Airplane," NACA WR L-86, 1945.

[5]Zalovcik, J. A. and Skoog, R. B., "Flight Investigation of Boundary-Layer Transition and Profile Drag of an Experimental Low-Drag Wing Installed on a Fighter-Type Airplane," NACA WR L-94, 1945.

[6]Holmes, B. J., Obara, C. J., and Yip, L. P., "Natural Laminar Flow Experiments on Modern Airplane Surfaces," NASA TP 2256, 1984.

[7]Miley, S. J., Howard, R. M., and Holmes, B. J., "Wing Laminar Boundary Layer in the Presence of a Propeller Slipstream," *Journal of Aircraft*, Vol. 25, July 1988, pp. 606–611.

[8]Schlichting, H., "Determination of Profile Drag," *Boundary-Layer Theory*, 6th ed., McGraw-Hill, New York, 1968, pp. 714–715.

[9]Johnson, D. K., "A Data Analysis System for Unsteady Turbulence Measurements," Masters Thesis, Naval Postgraduate School, Monterey, CA, Sept. 1988.

[10]Meier, H. U. and Kreplin, H.-P., "Influence of Freestream Turbulence on Boundary-Layer Development," *AIAA Journal*, Vol. 18, Jan. 1980, pp. 11–15.

[11]Howard, R. M., "An Investigation of the Effects of the Propeller Slipstream on a Wing Boundary Layer," Ph.D. Dissertation, Texas A&M Univ., College Station, TX, May 1987.

[12]Cebeci, T. and Carr, L. W., "A Computer Program for Calculating Laminar and Turbulent Boundary Layers for Two-Dimensional Time-Dependent Flows," NASA TM 78470, March 1978.